Asian Journal of Pharmaceutical Sciences 18 (2023) 100815

Available online at www.sciencedirect.com

ScienceDirect

journal homepage: www.elsevier.com/locate/AJPS

Original Research Paper

Corrugated surface microparticles with chitosan and levofloxacin for improved aerodynamic performance

Chang-Soo Han[a,1], *Ji-Hyun Kang*[a,b,1], *Eun hye Park*[a], *Hyo-Jung Lee*[a], *So-Jeong Jeong*[a], *Dong-Wook Kim*[c], *Chun-Woong Park*[a,*]

[a] *College of Pharmacy, Chungbuk National University, Cheongju 28160, Republic of Korea*
[b] *School of Pharmacy, Jeonbuk National University, Jeonju 54896, Republic of Korea*
[c] *College of Pharmacy, Wonkwang University, Iksan 54538, Republic of Korea*

ARTICLE INFO

Article history:
Received 15 November 2022
Revised 4 April 2023
Accepted 30 April 2023
Available online 21 May 2023

Keywords:
Chitosan
Organic acid
Levofloxacin
Corrugated surface
Aerodynamic performance

ABSTRACT

Corrugated surface microparticles comprising levofloxacin (LEV), chitosan and organic acid were prepared using the 3-combo spray drying method. The amount and the boiling point of the organic acid affected the degree of roughness. In this study, we tried to improve the aerodynamic performance and increase aerosolization by corrugated surface microparticle for lung drug delivery efficiency as dry powder inhaler. HMP175 L20 prepared with 175 mmol propionic acid solution was corrugated more than HMF175 L20 prepared with 175 mmol formic acid solution. The ACI and PIV results showed a significant increase in aerodynamic performance of corrugated microparticles. The FPF value of HMP175 L20 was 41.3% ± 3.9% compared with 25.6% ± 7.7% of HMF175 L20. Corrugated microparticles also showed better aerosolization, decreased x-axial velocity, and variable angle. Rapid dissolution of drug formulations was observed *in vivo*. Low doses administered to the lungs achieved higher LEV concentrations in the lung fluid than high doses administered orally. Surface modification in the polymer-based formulation was achieved by controlling the evaporation rate and improving the inhalation efficiency of DPIs.

1. Introduction

Dry powder inhalers (DPIs) are an attractive drug delivery method for the treatment of pulmonary diseases. DPIs are propellant-free, portable and physicochemically stable compared with other inhalers such as pressurized metered-dose inhaler, soft mist inhaler and nebulizer [1–4]. The inhalation efficiency of DPIs depends on aerosolization and pulmonary deposition of the formulation [5,6]. Novel inhaled particle, carriers and devices have been studied for increasing inhalation efficiency. This study investigated the enhanced

* Corresponding author.
E-mail address: cwpark@cbnu.ac.kr (C.-W. Park).
[1] These authors contributed equally to this work.
Peer review under responsibility of Shenyang Pharmaceutical University.

https://doi.org/10.1016/j.ajps.2023.100815

inhalation efficiency of corrugated surface of microparticles. Increased surface roughness in microparticles was shown to reduce particle-particle interaction and affect powder behavior in terms of particle velocity and direction upon delivery within the lung because of varying degrees of roughness [7,8]. Improved aerosolization and lung deposition due to surface roughness increases the inhalation efficiency [9–11]. The corrugated structure with rough surface can be prepared by controlling the evaporation rate in colloidal suspension [12–14].

The spray drying technique is a one-step continuous particle processing operation transforming a fluid state into a dry particulate form [15]. It is simple, scalable and cost-effective [16,17]. Spray drying of colloidal dispersion and controlled evaporation of particle-laden emulsions are used to create supra-colloids or micro-granules of controlled size, shape and morphonology [16,18]. In this study, the particle morphology was changed under constant drying conditions for application to other heat-sensitive drugs, by controlling the composition. Corrugated chitosan microparticle was prepared using a 3-combo spray drying method with colloidal chitosan, organic acid and levofloxacin HCl (LEV) for improved inhalation efficiency in DPI formulation. This study suggests that if the degree of corrugation of particles can be controlled by using organic acids with different boiling points, it would be possible to prepare corrugated particles at lower temperatures than previous studies and could have an impact on the aerosolization of particles, ultimately leading to improved inhalation efficiency [19,20].

Chitosan is a biocompatible and biodegradable polymer with low toxicity [21,22]. Moreover, it is mucoadhesive and promotes the diffusion of macromolecules through well-organized epithelial-like pulmonary layers [23–26]. It can easily dissolve in acid solution, and flexible particles of various shapes and surface properties can be prepared from dissolved chitosan colloidal solution [27]. Chitosan was selected as a polymer in this study because of its low toxicity, wide use in inhalant research, and easy particle shape modification.

Formic acid (FOR), acetic acid (ACE) and propionic acid (PRO) are volatile organic acids [28,29]. The boiling point increases with the increase in carbon number in the order of FOR (100.8 °C), ACE (118 °C) and PRO (141.2 °C). The different boiling point and concentrations of organic acid affect the evaporation rate in the spray drying process. As mentioned earlier, many efforts have been made to develop corrugated microparticles for DPI. However, there was no attempt to control the surface characteristics by varying the types and amounts of organic acids. We used organic acids as additives during spray drying, and the goal was to volatilize only some components (organic acids) with different boiling points from the particles to form a wrinkled structure under conditions of similar particle sizes and shape.

LEV is a third-generation fluoroquinolone antibiotic. It acts by inhibiting bacterial topoisomerase II, which is required for DNA replication, RNA transcription, and repair of bacterial DNA [30,31]. Inhalation of spray dried LEV has gained increasing attention in the treatment of pneumonia, chronic lung infection, and cystic fibrosis [32,33].

In this study, corrugated microparticles were successfully prepared using the 3-combo spray drying method containing polymers, organic acids and drugs. *In vitro* data showed that corrugated microparticles improved the aerodynamic performance and increased aerosolization as well as the amount of drug delivered deep inside the lung.

Table 1 – Formulations of prepared chitosan microparticles solution (HM: high-molecular weight chitosan; F: formic acid; A: acetic acid; P: propionic acid; L: levofloxacin).

Formulation	Chitosan (g/l)	Levofloxacin (g/l)	Acid type	Acid concentration (mmol/l)
HMF17.5 L0	5	0	FOR	17.5
HMF87.5 L0	5	0		87.5
HMF175 L0	5	0		175
HMA17.5 L0	5	0	ACE	17.5
HMA87.5 L0	5	0		87.5
HMA175 L0	5	0		175
HMP17.5 L0	5	0	PRO	17.5
HMP87.5 L0	5	0		87.5
HMP175 L0	5	0		175
HMP175 L1	5	0.05	PRO	175
HMP175 L10	5	0.5		
HMP175 L20	5	1		
HMP175 L30	5	1.5		
HMF175 L20	5	1	FOR	175

2. Materials and methods

2.1. Materials

LEV was provided by Huisun Pharma (Shaanxi, China). High-molecular weight (M.W.) chitosan (average M.W.: 310–375 kDa; degree of deacetylation: 75%) was supplied by Merck (Darmstadt, Germany). FOR was provided by Merck (Darmstadt, Germany). ACE and PRO were purchased from Dae Jung (Siheung, Korea). Methanol and acetonitrile (ACN) were of high-performance liquid chromatography (HPLC) grade and ordered from Honeywell Burdick & Jackson Ltd. (Muskegon, MI, USA). Other chemicals were of analytical grade and used as received. All experiments were carried out using Milli-Q® distilled water.

2.2. Preparation of corrugated microparticles

Corrugated microparticles were prepared via a 3-combo spray drying method with an organic acid, chitosan and drug using a laboratory scale spray dryer (Eyela SD-1000, Rikakikai Co. Ltd., Tokyo, Japan). The weights of chitosan and LEV are listed in Table 1. Chitosan was dissolved in organic acid solutions of different acid ratios (FOR, ACE and PRO at 17.5 mmol, 87.5 mmol and 175 mmol, respectively) and stirred for more than 12 h. LEV was added to chitosan solution to obtain the LEV-chitosan solution, which was spray-dried under the following conditions: inlet temperature of 160 °C; outlet temperature of 65–75 °C; nozzle size, 0.4 mm; feed rate, 6.5 ml/min; atomization air pressure,150 kPa; and

drying airflow rate, 0.30 m^3/min. The spray-dried corrugated microparticles were stored in a glass vial containing silica gel at −20 °C to prevent alteration of physicochemical properties.

2.3. Encapsulation efficiency and drug loading

The effect of HMF175 L20 and HMP175 L20 on the enpcasulation efficiency was determined according to the degree of wrinkles. The encapsulation efficiency was measured using a Waters Alliance 2695 HPLC system (Waters Corp., Milford, MA, USA) and, C_{18} column (5 µm, 100 Å, 250 mm × 4.6 mm) from Phenomenex Ltd (Torrance, CA, USA). The mobile phase consisting of ACN and buffer (0.04 M phosphoric acid, pH 4.0 adjusted with triethylamine) at a 15: 85 (v/v) ratio was eluted at a flow rate of 1.0 ml/min. The detection wavelength was set at 360 nm and the injection volume was 50 µl. The calibration curve was linear in the range of 0.63 to 25 µg/ml (r^2 = 0.99996) and 15 mg of prepared microparticles was dissolved in 50 ml mobile phase using Branson Model 8510® Ultrasonic Cleaner (Branson Ltd., Saint Louis, MO, USA) and filtered with a 0.2 µm PVDF-syringe filter (Hyundai micro Co., Ltd., Seoul, Korea). The entrapment efficiency (%) and drug loading (%) were calculated using Eqs. (1) and (2), respectively. All measurements were conducted in triplicate.

$$\text{Encapsulation efficiency (\%)} = \frac{\text{Amount of drug in microspheres}}{\text{Theoretical amount of drug}} \times 100\% \quad (1)$$

$$\text{Drug loading (\%)} = \frac{\text{Amount of drug encapsulated in microspheres}}{\text{Total amount of microspheres}} \times 100\% \quad (2)$$

2.4. Physicochemical properties of corrugated microparticles

2.4.1. Scanning electron microscopy

The scanning electron microscopic (SEM) images of prepared formulations were obtained using GEMINI LEO 1530® (Zeiss Ltd., Jena, Germany). Samples were mounted on an aluminum plate using carbon tape, then placed inside a Hummer VI sputtering device (Minneapolis, MN, USA), and coated with platinum to discharge the particles with 200 Å coating thickness. The magnification was × 20,000 or × 10,000. The voltage was 3 kV.

2.4.2. Atomic force microscopy

Atomic force microscopy (AFM, Dimension Icon, Bruker, Billerica, MA, USA) was used to analyze the surface topography of prepared microparticles. AFM images were acquired in the air and the conventional tapping mode. Samples were transferred onto carbon tape and scanned using PPP-NCLR-50 cantilevers (Nanosensors™, Neuchatel, Switzerland). The images were captured with a scan size 5 µm × 5 µm at a scan rate of 0.50 Hz. The images were analyzed using NanoScope Analysis 1.5 version software (Bruker). Root mean square roughness (R_{rms}) was calculated based on the AFM height deviation from the mean height value of each scan using Eq. (3) [34,35]. The "h" is the measured height, and "n" is the number of measurements.

$$\text{Rrms} = \sqrt{\frac{h_1^2 + h_2^2 + h_3^2 + \ldots + h_n^2}{n}} \quad (3)$$

2.4.3. Focused ion beam

Focused ion-beam (FIB) imaging was conducted in a Crossbeam 540 using gallium ions of 30 keV energy with beam currents of 1.5–7 nA for particle milling. Mechanical capabilities of the workstation include full in-plane rotation in addition to a 54° tilt. SEM imaging was performed by placing the sample on a carbon tape for platinum coating using a Hummer VI sputtering device, reaching 10 nm coating thickness. A voltage of 2 kV and a magnification of × 15,000 were used.

2.4.4. Particle size distribution

Corrugated microparticles were measured using laser diffraction particle sizing (Mastersizer 3000, Malvern, Worcestershire, UK).

2.4.5. True density and tapped density

A pycnometer (Ultrapyc 1200e, Quantachrome, Boynton Beach, FL, USA) was used to determine the true density of the corrugated microparticles under helium gas. The temperature was maintained at 20–21 °C, and each sample was run five times. Tapped density of corrugated microparticles was measured using 1 cc Luer-Lock syringe with a cap (BD Luer-Lok™, BD bioscience, Franklin Lakes, NJ, USA) containing a linear scale with 0.1 ml increments. The syringe with 100 mg the powder sample was then tapped manually on a flat workbench until the volume remained constant, and the volume was noted as the tapped volume.

2.4.6. Differential scanning calorimetry (DSC)

The thermal properties of sample were analyzed using a Q2000® (TA Instruments Ltd., New Castle, DE, USA). The samples were heated from 0 °C to 250 °C at a rate of 10 °C/min under a nitrogen flow of 50 ml/min.

2.4.7. Powder X-ray diffraction

The powder X-ray diffraction (PXRD) patterns of corrugated microparticles were measured using X'Pert PRO MRD® (PANalytical Ltd., Almelo, Netherlands) with Cu Kα radiation generated at 40 mA and 40 kV. The samples were placed on a silicon plate at room temperature, and 2θ scans were collected from 5° to 60°.

2.4.8. Fourier transformation-infra red

Fourier transformation-infra red (FTIR) spectroscopy of the prepared microparticles was performed in the range of 500 to 4000 cm^{-1} using Cary670 (Agilent, Santa Clara, CA, USA). The attenuated total reflectance (ATR) method was used with mercury cadmium telluride (MCT) detector. The spectral resolution is set 2.0 cm^{-1}.

2.5. In vitro *dissolution study using Franz diffusion cell system*

The *in vitro* dissolution profiles of corrugated microparticles as DPIs were investigated using a Franz diffusion cell system (FCDS-900C, Labfine Instruments, Gunpo, Korea). The medium reservoir of the Franz cell was filled with PBS buffer at pH 7.4 and maintained at 37 ± 1 °C. The medium was continuously stirred to ensure homogeneity. A regenerated cellulose membrane filter (pore size: 0.45 μm, GVS, Sanford, ME, USA) was then used as a barrier and placed in the membrane holder to facilitate contact with the medium. The sample was loaded on the membrane filter using a modified ACI system [36,37]. At the defined time, 200 μl samples were removed, and the same volume of fresh buffer was refilled to maintain a constant medium volume. The samples were centrifuged for 10 min at 1000 rpm to obtain the supernatant and their LEV content was measured using the modified HPLC method. All experiments were done with $n = 4$.

2.6. *Determination of aerosol dispersion performance using Andersen cascade impactor*

The aerosol performance of carrier-based formulations with RS01® device (Plastiape, Osnago, Italy) was evaluated using a carrier-based formulation and an 8-stage nonviable Anderson Cascade Impactor (ACI) (TE-20–800, TISCH Environmental Inc., Cleves, OH, USA), based on USP Chapter <601> specification for aerosols. A flow rate of 60 l/min was set and confirmed before each experiment using a flow meter (DFM 2000, COPLEY scientific, Nottingham, Nottinghamshire, UK). The ACI stage collection plates were coated with silicone oil to prevent particle bounce and re-entrainment during the test. Number 3 gelatin capsules were manually filled with 20 mg prepared formulations. The mouthpiece was mounted in an induction port with inserted devices. Experiments were performed at a flow rate of 60 l/min for 4 s controlled by a flow controller (TPK-R™, COPLEY scientific). The drug amount remaining in the capsule and deposited onto the collection plate of each state was quantified using modified HPLC methods. The aerodynamic cut-off diameters of each stage were 8.6 μm, 6.5 μm, 4.4 μm, 3.3 μm, 2.0 μm, 1.1 μm, 0.54 μm and 0.25 μm for stages −1, 0, 1, 2, 3, 4, 5, and 6, respectively, at a flow rate of 60 l/min [38]. The emitted dose (ED) represented the percentage of the difference between the initial and the residual weights of the drug in the capsule after aerosolization. The respiratory dose was defined as the amount of drug deposited in stages 1 through 6. The fine particle fraction (FPF) indicated the particle ability to reach the respirable region with an aerodynamic size of about 5.0 μm or less. FPF is expressed as the proportion of drug collected at stages 1 through 6 in the ED based on the Eqs. (4) and (5) below.

$$\text{Emitted dose (\%)} = \frac{\text{The total dose in capsules} - \text{Drug amount remaining in the capsule}}{\text{The total dose in capsules}} \times 100\% \quad (4)$$

$$\text{Fine particle fraction (\%)} = \frac{\text{Total drug amount on stages 1 through 6}}{\text{Total drug amount on all stages}} \times 100\% \quad (5)$$

The mass median aerodynamic diameter (MMAD) and geometric standard deviation (GSD) were calculated from the drug mass deposited on the ACI stages. All experiments were done in triplicate.

2.7. *Aerosol dispersion performance based on particle image velocimetry*

Particle Image Velocimetry (PIV) system and grid design were set up similarly to the reference [8]. Prepared formulations (20 mg each) were added to the #3 gelatin capsule. RS01® device (Plastiape, Osnago, Italy) mounted in a clear acrylic cube (200 × 200 × 200 mm). The flow rate of 28.3 l/min [39] was obtained using a vacuum pump (Edwards, Burgess Hill, West Sussex, UK). The 5.5-mV laser sheet beam (Specification, 532 nm) was created parallel to the device with a diode laser (Laserlab, Yongin, Korea). The images of particle behavior were measured at 8.000 frames/s and a resolution of 640 × 480 pixels using a high-speed camera (HAS-D71M, DITECT Corporation, Tokyo, Japan) positioned perpendicular to the laser sheet plane. The chamber was divided into 50 × 50 grids, and images were processed with a PIV analysis software (Flownizer 2D ver1.2.1.2, DITECT Corporation). Particle velocities (8, 25) were determined in the images between two frames using the combined algorithm of recursive cross-correlation. All experiments were done in triplicate.

2.8. In vivo *evaluation of corrugated microparticles*

2.8.1. *Pharmacokinetic study in plasma*

Animals were treated and maintained in accordance with the principles of laboratory animal care and approved by the Committee for Animal Experiments of Chungbuk National University (Cheongju, Korea). Sprague Dawley® rats (male, 250–300 g) were purchased from Samtako Bio Korea (Osan, Korea) and fed *ad libitum*. The rats were randomly divided into four groups. The oral group (Oral-Sol (15.0mpk) group) received 15 mg/kg dose, and the other groups received 1.5 mg/kg doses delivered via lung. All groups were anesthetized using isoflurane. The oral group ($n = 3$) was treated with 3 mg/ml LEV solution using 18 G oral gavage. Rats in the intratracheal instillation group (ITI-Sol (1.5mpk) group) were treated with 1.5 mg/ml LEV solution using a MicroSpray aerosolizer (BJ-PW-R, BioJane, Shanghai, China). HMP175 L20 (ITI-HMP (1.5mpk) group) and HMF175 L20 (ITI-HMF (1.5mpk) group) were administered with dry powder using an insufflator (BJ-PW-FM-R, BioJane). Blood samples (400 μl) were collected into EDTA microcontainer tubes (BD Science) at predetermined time points (0.167, 0.333, 0.5, 0.75, 1, 1.5, 2, 3, and 6 h) after administration. Plasma

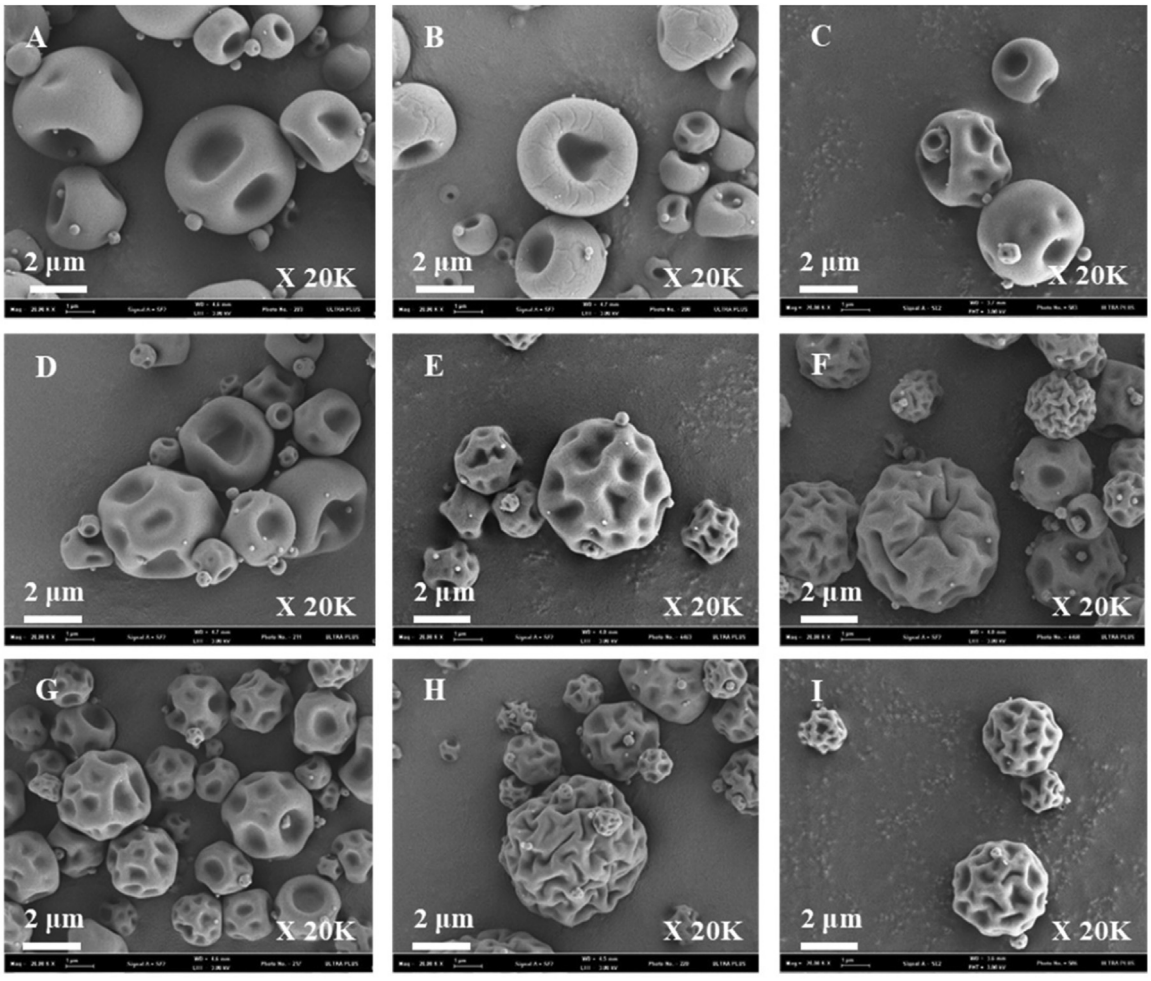

Fig. 1 – SEM images of corrugated microparticle according to weight ratios of each organic acids. (A) HMF17.5 L0, (B) HMF87.5 L0, (C) HMF175 L0, (D) HMA17.5 L0, (E) HMA87.5 L0, (F) HMA175 L0, (G) HMP17.5 L0, (H) HMP87.5 L0 and (I) HMP175 L0.

was immediately separated via centrifugation and stored at – 80 °C until analysis. Plasma samples were analyzed using an in-house HPLC fluorescence method (HPLC-FLD). Chromatographic separation was carried out on an Aegispak C_{18}-L column (150 mm × 4.6 mm, 5 µm; Young Jin Biochrom co., Ltd, Seongnam, Korea). The temperature of the column oven was maintained at 35 °C during the analysis. The isocratic mobile phase included a mixture of 0.4% aqueous triethylamine (pH adjusted to 3.0 with phosphoric acid)-methanol-acetonitrile (75: 22.5:2.5,v/v), which was pumped at a flow rate of 1.0 ml/min, followed by detection with an Agilent 1200 fluorescence detector ($\lambda_{excitation}$= 292 nm, $\lambda_{emission}$= 494 nm). Data acquisition and integration were performed using Agilent ChemStation b.04.03 software.

2.8.2. *Bronchoalveolar lavage fluid concentration*

The rats were randomly divided into four groups and treated with a dose of 15 mg/kg or 1.5 mg/kg as described in Section 2.8.1. The rats were sacrificed at predetermined time points (10, 20, and 30 min) after administration. The lungs were collected, and the bronchoalveolar lavage fluid (BALF) was sampled by gently and repeatedly flushing with saline five times using a plunger. The BALF samples were immediately separated via centrifugation and stored at - 80 °C until analysis. The BALF samples were assayed using a valid HPLC-FLD, as described in Section 2.8.1.

2.9. *Statistical analysis*

All statistical analyses were conducted using the one-way analysis of variance (ANOVA) or t-test with GraphPad Prism 8 (release 8.4.2, San Diego, CA, USA). *P*-values smaller than 0.05 were considered statistically significant.

3. Results and discussion

3.1. *Particle and surface morphology of corrugated microparticles*

3.1.1. *SEM*

Corrugated chitosan microparticles were prepared via spray drying method. All prepared powder formulations were pale beige in color. The SEM images of prepared formulations according to weight ratios of each organic acid in the spray drying method are shown in Fig. 1. The number

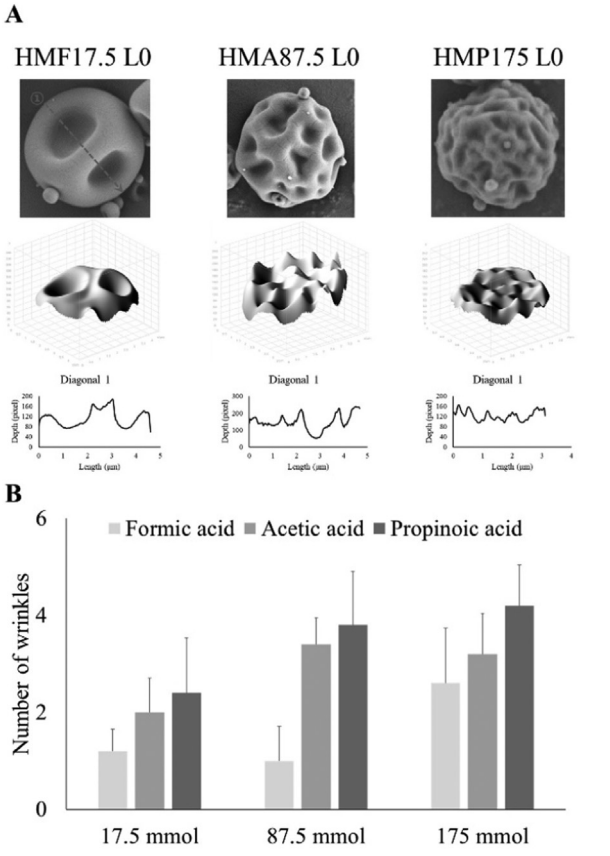

Fig. 2 – Imaging analysis of corrugated microparticles using Image J software. (A) Images of corrugated microparticles. (B) Relationship between the weight ratio of each organic acid and wrinkles (n = 3).

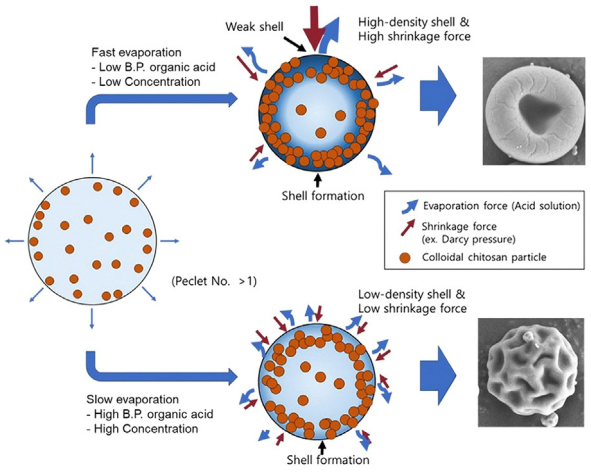

Fig. 3 – Schematic diagram of corrugated microparticle formation with different organic acid.

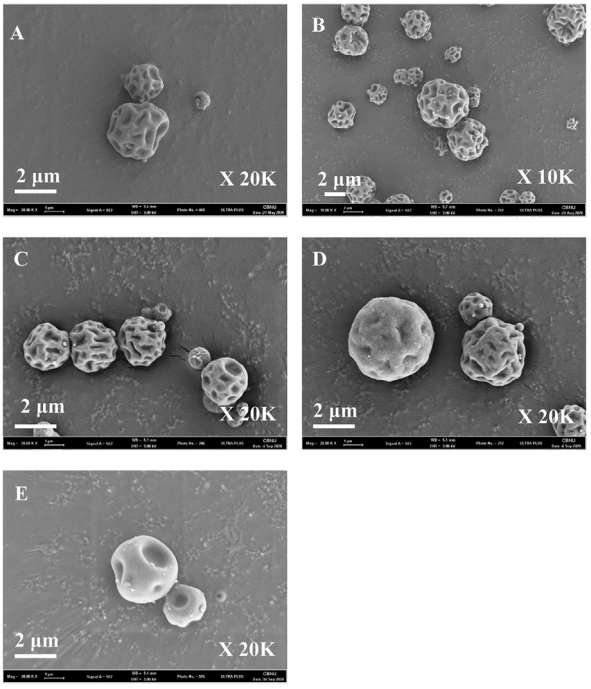

Fig. 4 – SEM images of corrugated microparticle according to chitosan and levofloxacin HCl ratio in propionic acid 175 mmol. (A) HMP175 L1, (B) HMP175 L10, (C) HMP175 L20, (D) HMP175 L30, and (E) HMF175 L20.

of wrinkles in SEM images were measured using Image J (National Institutes of Health, Bethesda, MD, USA), as shown in Fig. 2. The wrinkle structure in the microparticles was increased as the boiling point of organic acid increased in the order of formic acid (HMF), acetic acid (HMA), and propionic acid (HMP). Additional corrugated structures were observed at high concentrations of 175 mmol with all types of acid (HMF175 L0, HMA175 L0, and HMP175 L0). Corrugated microparticle surfaces can be obtained by controlling the rate of surface formation in colloidal solution. The rate of surface formation during particle drying is affected by the boiling point and concentration of organic acid required to dissolve the chitosan. PRO with larger molecular weight had a higher boiling point resulting in slow shell formation during particle drying than FOR and ACE (Fig. 3). Because the Peclet number is also the largest for propionic acid, more wrinkled structures are created [40]. Slow drying formulations lead to the formation of less dense shells compared to fast drying formulations. Vapor evaporated from the inside escapes through the formed shell, creating a contractile force such as Darcy friction [16,41]. In the case of FOR, a highly dense shell is formed, which does not allow for easy vapor evaporation, resulting in high vapor pressure. The high vapor pressure emerges from weak spots in the shell, resulting in the formation of particles with large grooves. On the other hand, a loosened shell formed by ACE and PRO allows steam to pass between the shells, and the resulting Darcy friction generates shrinkage evenly, leading to the formation of wrinkled microparticles [42,43]. In summary, the degree of wrinkling of the chitosan microparticles increased with higher organic acid concentrations and boiling points under the same spray-drying conditions. The effect of LEV ratio on HMP175 formulations was evaluated as shown in Fig. 4. As the effect of LEV was not observed up to a 20% ratio on the formation of wrinkles. Particles with uniform roughness until 20% compared with chitosan were obtained. HMP175 L30 showed corrugated structures, but a non-uniform shape

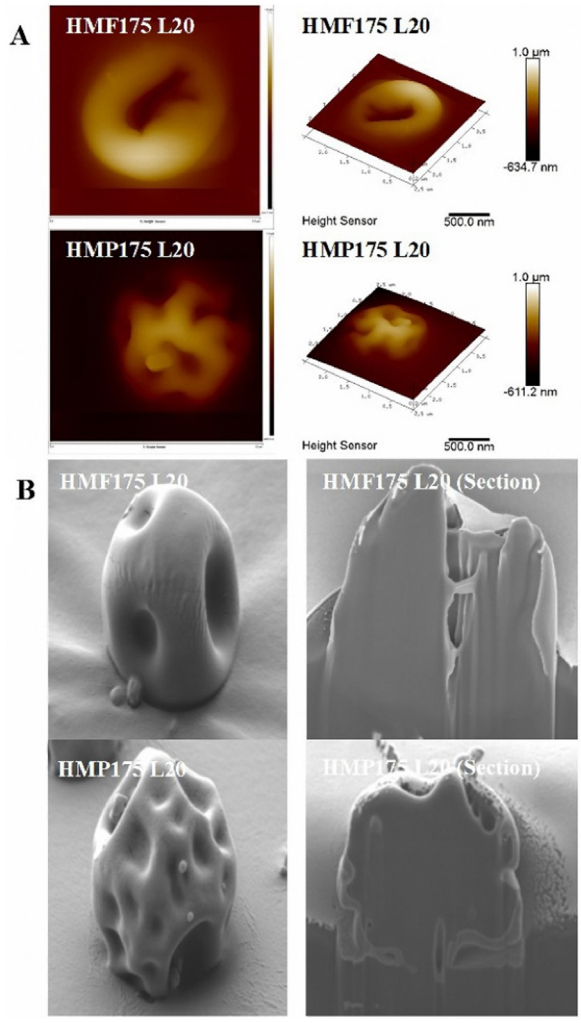

Fig. 5 – Atomic force microscopy and focused ion beam-SEM images of HMF175 L20 and HMP175 L20; (A) Surface roughness images obtained by AFM. (B) Sectioned microparticle images.

was obtained. A high concentration of drug affected the shell formation by increasing the boiling point of the organic acid solution with boiling point evaluation. The formulation using FOR was prepared with a 20% drug ratio and resulted in a uniformly wrinkled shape with a single large wrinkle.

3.1.2. Surface topography and section of corrugated microparticle

The surface topography of corrugated microparticles was analyzed via AFM. The representative images of HMF175 L20 and HMP175 L20 are shown in Fig. 5, and the roughness of the prepared formulations is shown in Table 2. HMP175 L20 with PRO was associated with significantly more numerous ($P = 0.005$) and deeper wrinkles ($P = 0.006$) than HMF175 L20 withFOR. The root mean square value was calculated in the surface roughness of the particles. The R_{rms} value of HMF175 L20 was 569.88 nm, which is higher than 273.61 nm of HMP175 L20. The larger R_{rms} value of HMF175 L20 was attributed to a large amount of vapor emitted at one spot, resulting in large structural collapse. In addition, there were no significant differences in true density or tapped density, suggesting that particle packing does not vary depending on the size or shape of wrinkles.

Table 2 – Void volume, depth, density, and entrapment efficiency of the drug release of HMF175 L20 and HMP175 L20 (mean ± SD).

Formulation	HMF175 L20	HMP175 L20
Dv10 (µm, $n = 3$)	0.436 ± 0.001	0.425 ± 0.001
Dv50 (µm, $n = 3$)	3.135 ± 0.035	3.000 ± 0.014
Dv90 (µm, $n = 3$)	6.135 ± 0.304	5.635 ± 0.007
Span ($n = 3$)	1.816 ± 0.076	1.736 ± 0.005
Wrinkles ($n = 3$)	1.33 ± 0.58	8.00 ± 1.00
Depth (nm) ($n = 3$)	566.3 ± 77.7	266.7 ± 67.1
R_{rms} (nm)	569.88	273.61
True density (g/cc, $n = 5$)	1.561 ± 0.001	1.455 ± 0.001
Tapped density (g/cc, $n = 3$)	0.562 ± 0.040	0.670 ± 0.020
Entrapment efficiency (%, $n = 3$)	82.34 ± 0.94	83.26 ± 1.38
Drug loading amount (%, $n = 3$)	13.72 ± 0.16	13.88 ± 0.23

*$P < 0.05$, ** $P < 0.01$, ***$P < 0.001$ Compared with HMF175 L20 (t-test)

The prepared microparticles were sectioned using FIB system. Cross-sectional images of corrugated microparticles are presented in Fig. 5. Shell formation and cavities were observed. It is called a wrinkled surface because it is not a pore structure in which holes are connected to the inside like channel [44]. HMF175 L20 was prepared with FOR showed larger cavities than HMP175 L20 with propionic acid. Cavities around the corrugated structure suggested traces of vapor emission [45]. The observed shells and cavities of formulations explain the mechanism of corrugated structure formation during spray drying.

3.2. Physicochemical properties of corrugated microparticles

3.2.1. Particle size distribution

The particle size distribution of the prepared formulations is presented in Table 2. All formulations showed similar Dv_{50} values within the range of 2.7 to 3.3 µm. All prepared microparticles showed similar size distribution regardless of formulations and the measurements matched with the SEM image parameters appropriate for dry powder inhalation.

3.2.2. True density, tapped density, and entrapment efficiency

The results of true density, tapped density and drug entrapment efficiency are shown in Table 2. The true densities of HMF175 L20 and HMP175 L20 were 1.561 ± 0.001 and 1.455 ± 0.001 g/cc, respectively, suggesting the presence of similar components. So, the difference of true density between these formulations would not have a significant impact on the inhalation efficiency. The tapped densities of HMF175 L20 and HMP175 L20 were 0.562 ± 0.040 and 0.670 ± 0.020 g/cc, respectively. The tapped density of the formulations prepared with PRO was higher than that of the formulations prepared with FOR. Corrugated microparticles have higher tapped density than smooth surface microparticle due to particle interlocking, which

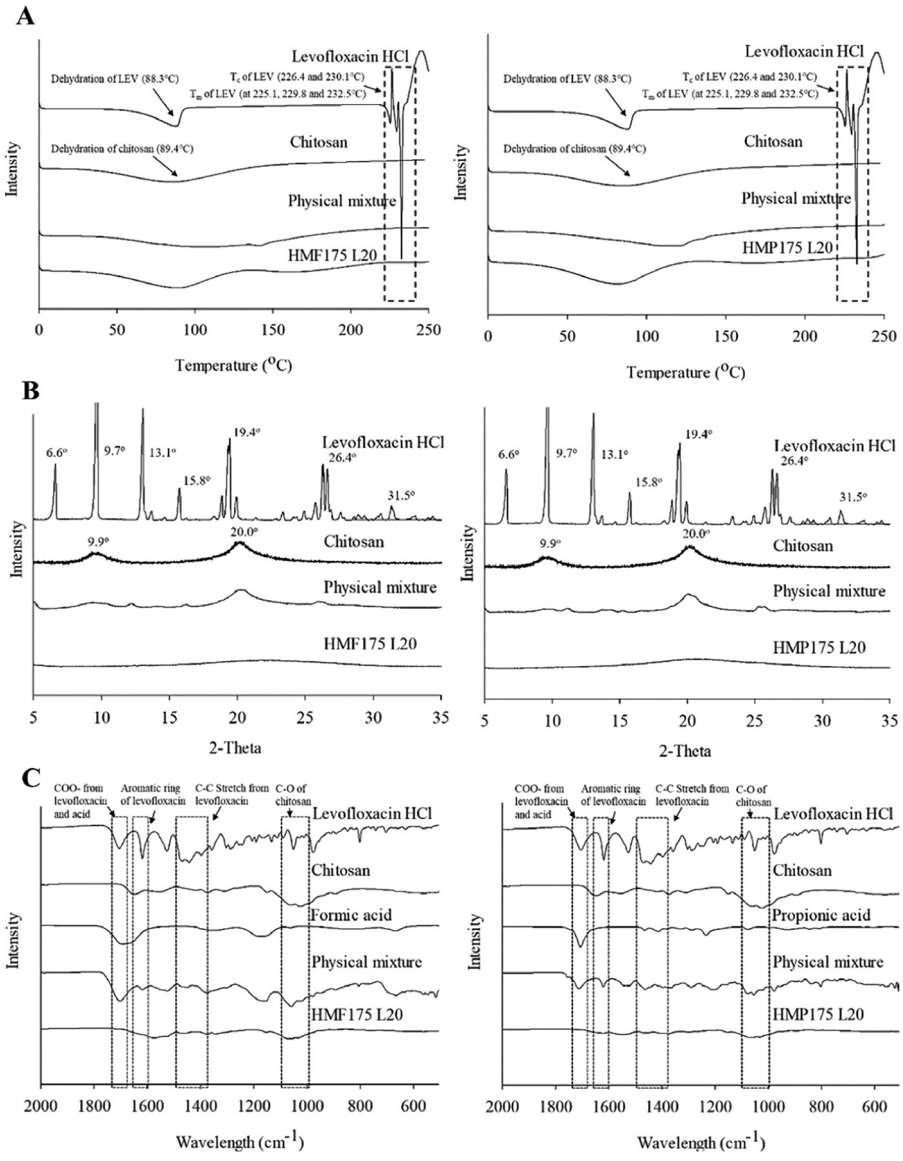

Fig. 6 – Physicochemical property characterization of HMF175 L20 and HMP175 L20. (A) DSC, (B) XRD, and (C) FTIR results of HMF175 L20 and HMP175 L20.

reduces interparticle voids, and leads to tight packing and increased tapped density [46,47]. The entrapment efficiency of HMF175 L20 and HMP175 L20 were 82.34% ± 0.94% and 83.26% ± 1.38%.

3.2.3. *DSC, XRD and FTIR*

The DSC, XRD and FTIR results of HMF175 L20 and HMP175 L20 are shown in Fig. 6. Dehydration of LEV was observed around 100 °C, and the melting point (Tm) of LEV was confirmed at 220–240 °C with recrystallization [48]. Chitosan presented a dehydration peak around 90 °C and the Tm was not observed due to polymer properties [49]. The physical mixture showed a similar peak pattern compared to chitosan, and no drug-derived Tc and Tm were observed due to the dilution of chitosan. All formulations showed endothermic peaks that were dehydrated around 100 °C and presented a similar thermogram pattern with a chitosan-like composition due to the dilution effect.

LEV showed sharp and strong diffraction peaks at 6.6°, 9.7°, 13.1°, 15.8°, 19.4°, 26.4°and 31.5°, and high-molecular weight chitosan showed broad peaks around 10° and 20° [50,51]. None of the prepared formulations showed crystalline chitosan or LEV, which were transformed into amorphous powder by the spray- drying process. The drug was dispersed in the polymer matrix and maintained in an amorphous state, which improved the bioavailability and dissolution rate [52].

LEV showed the peak of C–O stretching vibration of the COOH group at 1725 cm^{-1}, a 1620 cm^{-1} peak for aromatic rings, and a 1500–1400 cm^{-1} broad peak for C–C [45]. Chitosan presented C–O stretching and bond at 1030 cm^{-1} [53]. Organic acid showed a 1725 cm^{-1} peak for the C–O stretching vibration of the COOH group. The physical mixture showed C–O

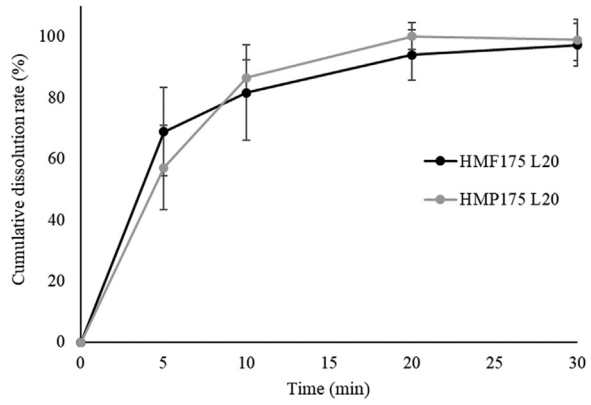

Fig. 7 – Dissolution profiles of HMF175 L20 and HMP175 L20 ($n = 3$).

stretching vibration of the COOH group at 1725 cm^{-1} in LEV and organic acids, and C–O stretching and bond at 1030 cm^{-1}. All prepared formulations showed similar FTIR results of the physical mixture except for the 1725 cm^{-1} peak of the COOH group. No major shift in the characteristic peaks was detected in the spectrum of the microparticles.

Overall, the results of DSC, XRD, and FTIR analyses suggest that LEV present in HMF175 L20 and HMP175 L20 exists in the amorphous form.

3.3. *Dissolution profiles of corrugated microparticles*

The dissolution of the prepared formulation was evaluated using the Franz cell ($n = 4$). Dissolution profiles are shown in Fig. 7. The time required for 90% of the drug release was within 20 min in both HMF175 L20 and HMP175 L20 and fully released within 30 min in the Franz cell. There was no significant difference in dissolution based on the structure of the wrinkles, possibly due to the high drug solubility and amorphous state in the formulations [54,55]. This result is similar to the previous findings from DSC, XRD and FTIR analyses, which showed that LEV exists in an amorphous state. Since there is no difference in dissolution between the two formulations, bioavailability is expected to vary only with the number of particles that reach the lungs.

The rapid drug release during dissolution suggests that the prepared formulations also released the drug rapidly even when it is administrated into the lung, which facilitated accumulation of lethal antibiotic concentrations required to kill bacteria [56].

3.4. In vitro *aerosol dispersion performance*

3.4.1. *Andersen cascade impactor*

The aerosol performance characteristics of HMF175 L20 and HMP175 L20 were evaluated using an ACI coupled with RS01® DPI device. The parameters related to aerodynamic performance are shown in Table 3. The emitted dose (ED) values for all samples were in the high range (90.9% to 95.3%). The respiratory dose of HMF175 L20, representing deposition in stages 1 through 6, was 0.71 ± 0.19, while that of HMP175 L20 was 1.17 ± 0.01, indicating a statistically significant difference. The HMF175 L20 exhibited 25.6% ± 7.7% of FPF (< 4.4 μm), with a MMAD of 2.4 ± 0.1 μm, and a GSD of 3.0 ± 0.1. The HMP175 L20 showed a FPF (< 4.4 μm) of 41.3% ± 3.9%, a MMAD of 2.2 ± 0.0 μm, and a GSD of 2.8 ± 0.0. HMP175 L20 carrying additional wrinkled structures exhibited better aerodynamic performance than HMF175 L20, which showed less wrinkled structure, suggesting that HMP175 L20 can be delivered more than HMF175 L20. HMP175 L20 showed significant improvement in FPF, MMAD and GSD values compared with HMF175 L20. ($P = 0.0372$ in FPF (< 4.4 μm), $P = 0.0071$ in MMAD, $P = 0.0273$ in GSD, t-test). In particular, the corrugated structure on microparticles yielded significantly higher values at the lower cut-off of FPF values representing the deeper lung ($P = 0.0096$ in FPF (< 3.2 μm), $P = 0.0035$ in FPF (< 1.2 μm), t-test). Based on the results presented in Table 2, we can infer that the reduction in particle-substrate interaction to facilitate aerosolization is a more significant factor than the packing effect caused by wrinkles. Thus, the FPF value is increased as the degree of wrinkles increased and facilitates drug delivery deep inside the lungs, contributing to the therapeutic effect [57].

Table 3 – Inhalation efficiency of HMF175 L20 and HMP175 L20 formulation by Andersen cascade impactor ($n = 3$, mean ± SD).

Formulation	HMF175 L20	HMP175 L20
ED (%)	93.4 ± 2.7	95.3 ± 2.8
Respiratory dose (<4.4 μm, mg)	0.71 ± 0.19	1.17 ± 0.01*
FPF (<4.4 μm,%)	25.6 ± 7.7	41.3 ± 3.9*
FPF (<3.2 μm,%)	15.4 ± 3.0	26.7 ± 2.9**
FPF (<1.2 μm,%)	9.5 ± 1.6	16.1 ± 0.9**
MMAD (μm)	2.4 ± 0.1	2.2 ± 0.0**
GSD	3.0 ± 0.1	2.8 ± 0.0*

*$P < 0.05$,**$P < 0.01$, ***$P < 0.001$ Compared with HMF175 L20 (t-test).

3.4.2. *Particle image velocimetry*

The aerosolization of particle was observed and the particle movement through the position (8, 25) in 50 × 50 grids was quantified via PIV analysis using Flownizer 2D ver1.2.1.2, as shown in Fig. 8. The HMP175 L20 was shown less agglomerated movement than HMF175 L20 in captured images. It is thought that aerosolization occurred better in HMP175 L20 due to nanoscale corrugated wrinkles [58,59].

The x-axial speed of HMF175 L20 was 4.46 ± 0.02 mm/ms, and the y-axial speed was 0.49 ± 0.01 mm/ms, with an angle of 7.29 ± 0.10° The x-axial speed, y-axial speed and angle of HMP175 L20 were 4.11 ± 0.02 mm/ms, 0.55 ± 0.01 mm/ms, and 9.45 ± 0.14°, respectively. HMP175 L20, which had a more wrinkled structure, showed significantly lower x-axial speed ($P < 0.0001$), higher y-axial speed ($P < 0.0001$), and increased variable angle ($P < 0.0001$). The y-axial value was very low compared with x-axial speed, and the improved aerodynamic performance based on FPF value, MMAD and GSD was attributed to x-axial speed. The x-axial speed and the angular diversity in PIV follow the similar trends as the FPF value based on the ACI results and the degree of wrinkles based on AFM results. It was confirmed that the

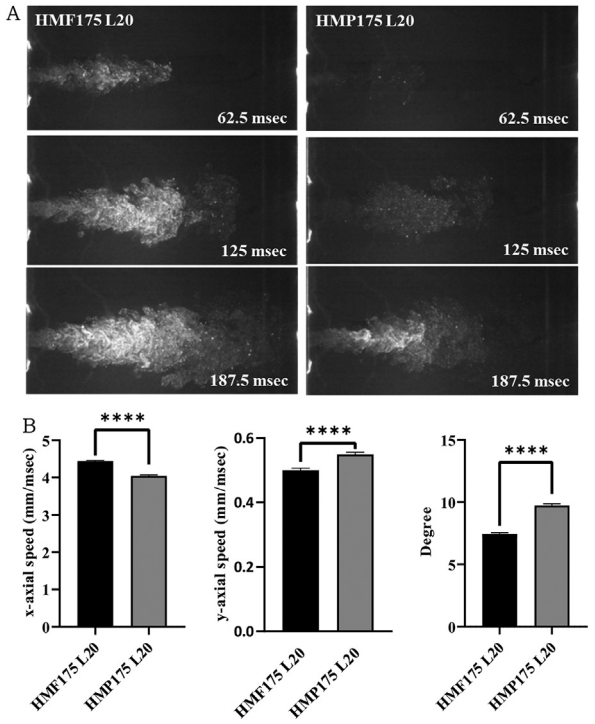

Fig. 8 – Aerodynamic performance of HMF175 L20 and HMP175 L20. (A) PIV images of HMF175 L20 and HMP175 L20 at 62.5 ms, 125 ms and 187.5 ms, and (B) PIV results of HMF175 L20 and HMP175 L20 ($n = 3$) *P < 0.05, **P < 0.01, ***P < 0.001, ****P < 0.0001 Compared with HMF175 L20 (t-test).

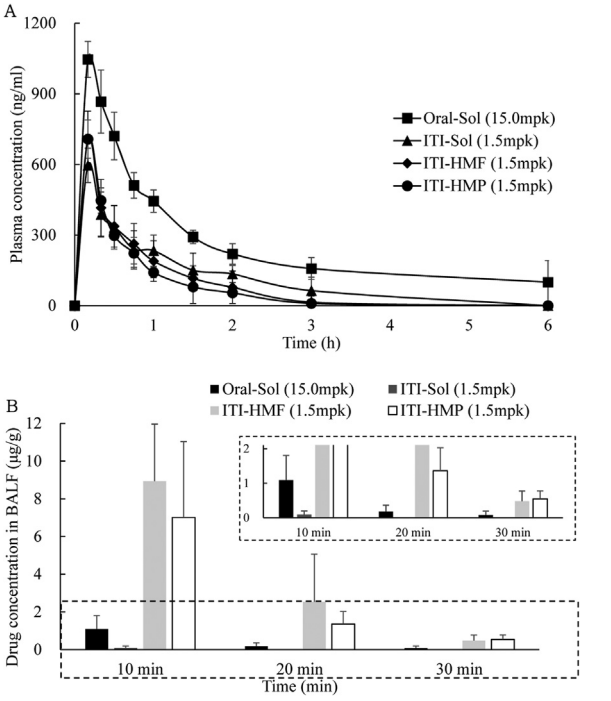

Fig. 9 – (A) Drug concentration in plasma after administration ($n = 3$), (B) Drug concentration in BALF after administration ($n = 3$ or 6).

microparticle wrinkle structure reduced the x-axial speed and diversified the movement of particles in the fluid. The reason is that the drag coefficient varies depending on the surface [60,61]. Accordingly, the particle removal rate by impaction in the oral mucosa at the beginning of inhalation could be reduced, and additional particles delivered to the deep lung [8,62].

3.5. In vivo test

3.5.1. *Pharmacokinetics of corrugated microparticles*

LEV solution was administrated at 1.5 mg/kg using a syringe-operated micro-cannula (ITI-Sol (1.5mpk) group). HMP175 L20 or HMF175 L20 was administrated at 1.5 mg/kg as a dry powdered using insufflator (ITI-HMP (1.5mpk) or ITI-HMF (1.5mpk) group). The drug was administered at a dose of 15 mg/kg orally (Oral-Sol (15.0mpk) group), which is a 10-fold increase in dose level compared with other routes of administration. It was difficult to confirm the pharmacokinetic (PK) profiles, such as the C_{max} of the drug, when administered via the lung route at similar doses, due to the difference in the degree of protein binding and absorption according to the route of administration of LEV in rats [63,64].

Pharmacokinetic profiles of LEV are presented in Fig. 9. and the parameters are shown in Table 4. A low bioavailability of the orally administered drug was confirmed in the rat. Comparing the AUC_{0-6hr} of plasma concentration, it was observed that the groups receiving direct lung administration exhibited three-fold higher absorption compared to the orally administered group. The AUC_{0-6hr}, C_{max}, T_{max} and $T_{1/2}$ values of ITI-HMP (1.5mpk) group were similar to those of ITI-Sol (1.5mpk) and ITI-HMF (1.5mpk) group. There was no significant difference between the ITI-HMP (1.5mpk) group and the ITI-HMF (1.5mpk) group. The reason is that the aerosol characteristics were not reflected because it was administered via intubation into the airway. Additionally, we were unable to confirm any impact of the wrinkle morphology on absorption mechanisms such as cell membrane penetration. The results suggest that the prepared HMP175 L20 and HMF175 L20 particles dissolved rapidly in the lungs of rats within 30 min under reduced water levels based on Franz cell dissolution studies. The rapid dissolution is attributed to the solubility of the drug and its amorphous state, and is expected to increase the concentration of antibiotics locally for rapid onset.

3.5.2. *BALF and lung distribution of corrugated microparticles*

LEV was administered at 15 mg/kg orally and at 1.5 mg/kg by ITI and Insufflator (Oral-Sol (15.0mpk) and ITI-Sol (1.5mpk): $n = 4$; ITI-HMP (1.5mpk) and ITI-HMF (1.5mpk): $n = 6$). The concentrations of LEV in BALF are shown in Fig. 9. It was expressed as the amount of drug (μg) per lung weight (g). After oral administration of 10-fold higher levels of drug, the LEV concentration in BALF (1.90 ± 0.71 μg/ml) above minimum inhibitory concentration of *Pseudomonas pneumoniae* (1 μg/ml) was barely maintained for 10 min. BALF concentrations in ITI-Sol (1.5mpk) were 0.09 ± 0.01 μg/ml at 10 min. Compared with Oral-Sol (15.0mpk) group, ITI-HMP (1.5mpk) and ITI-HMF (1.5mpk) groups were observed in BALF at high concentrations

Table 4 – PK parameters of Oral-Sol (15.0mpk), ITI-Sol (1.5mpk), ITI-HMF (1.5mpk), and ITI-HMP (1.5mpk) group. (n = 3, mean ± SD).

Parameter	Oral-Sol (15.0mpk)	ITI-Sol (1.5mpk)	ITI-HMF (1.5mpk)	ITI-HMP (1.5mpk)
Dose (mg/kg)	15	1.5	1.5	1.5
$AUC_{0-6\ h}$ (ng/ml·h)	1541.22 ± 9.65	685.52 ± 175.78**	542.07 ± 171.16*	464.62 ± 21.39*
C_{max} (ng/ml)	1046.34 ± 76.82	596.04 ± 73.01***	708.71 ± 118.23***	707.86 ± 81.37***
T_{max} (h)	0.17 ± 0.00	0.17 ± 0.00	0.17 ± 0.00	0.17 ± 0.00
$T_{1/2}$ (h)	0.65 ± 0.08	0.47 ± 0.10	0.37 ± 0.09	0.35 ± 0.11

*$P < 0.05$, **$P < 0.005$, ***$P < 0.0005$ Compared with Oral-Sol (15.0 mpk) group (ANOVA).

(7.01 ± 4.03 and 8.93 ± 3.03 μg/ml at 10 min; 1.36 ± 0.67 and 2.53 ± 2.53 μg/ml at 20 min) above the minimal inhibitory levels for 20 min. The concentration in BALF of ITI-HMF (1.5mpk) group has similar result with that of ITI-HMP (1.5mpk) group. This is because, as mentioned above, the aerosol characteristics were not reflected because the administration was intubated into the airway. The results showed that, with lung delivery, higher drug concentrations were detected in the lungs even with one-tenth the dose of oral administration, indicating that the maximum bactericidal effect on cystic fibrosis (CF) occurred within 10 min of exposure. Antimicrobial susceptibility studies of rapid and topical dissolution of the drug at high concentrations can benefit patients diagnosed with infectious diseases such as CF without adverse systemic effects [65,66]. The affinity of chitosan to mucus and dissolution time may contribute to maintenance of drug levels at higher concentrations in the lung and BALF locally compared with ITI. The delivery of LEV-chitosan microparticles to the lungs increases drug concentration locally at small doses.

4. Conclusion

Corrugated microparticles were prepared using the 3-combo spray-drying method, consisting of LEV, chitosan and organic acid. The increased weight and concentration of organic acid increased the number of wrinkles in microparticles in high-molecular chitosan. The wrinkled microparticle structure for dry powder inhalation resulted in improved inhalation efficiency, which was related to therapeutic effectiveness. Increased FPF, decreased MMAD, and decreased GSD values were evaluated in wrinkled microparticles prepared with PRO instead of those with fewer wrinkles obtained with FOR. PIV results showed that wrinkled particles traveled in fluid with reduced linearity and variable angle, and were expected to minimize the loss of particle impaction to oral mucus. *In vivo* testing revealed rapid drug release by chitosan microparticles from the mucous layer similar to the results of dissolution from Franz cell. Further studies on toxicity and stability are needed, and optimization of formulations and manufacturing processes for non-clinical studies is also needed in the future. In conclusion, the prepared particles ensured high concentrations of antibiotics in the lung mucosa even with low levels of drug, which had a positive impact on pulmonary infections such as CF. Wrinkled chitosan microparticles prepared by controlling organic acid represents a potential micro-carrier for DPIs with improved inhalation efficiency and dissolution profiles.

Conflicts of interest

The authors declare that they have no conflicts of interest.

Acknowledgement

This study was supported by a National Research Foundation of Korea grant provided by the Korean government (NRF-2021R1A2C4002746 and 2017R1A5A2015541). This research was supported by "Regional Innovation Strategy (RIS)" through the National Research Foundation of Korea (NRF) funded by the Ministry of Education (MOE)(2021RIS-001). Finally, this work was supported by a funding for the academic research program of Chungbuk National University in 2022.

Supplementary materials

Supplementary material associated with this article can be found, in the online version, at doi:10.1016/j.ajps.2023.100815.

References

[1] Chan HK. Inhalation drug delivery devices and emerging technologies. Expert Opin Ther Pat 2003;13(9):1333–43.
[2] Lavorini F, Pistolesi M, Usmani OS. Recent advances in capsule-based dry powder inhaler technology. Multidiscip Respir Med 2017;12:1–7.
[3] Mehta P. Dry powder inhalers: a focus on advancements in novel drug delivery systems. J Drug Deliv 2016:8290963 2016.
[4] Peng T, Lin S, Niu B, Wang X, Huang Y, Zhang X, et al. Influence of physical properties of carrier on the performance of dry powder inhalers. Acta Pharmaceutica Sinica B 2016;6(4):308–18.
[5] Dhand R. Inhaled drug therapy 2016: the year in review. Respir Care 2017;62(7):978–96.
[6] Price DN, Kunda NK, Muttil P. Challenges associated with the pulmonary delivery of therapeutic dry powders for preclinical testing. KONA Powder Part J 2019;36:129–44.
[7] Cheng W, Dunn PF, Brach RM. Surface roughness effects onmicroparticle adhesion. J Adhes 2002;78(11):929–65.

[8] Kwon YB, Kang JH, Han CS, Kim DW, Park CW. The effect of particle size and surface roughness of spray-dried bosentan microparticles on aerodynamic performance for dry powder inhalation. Pharmaceutics 2020;12(8):765.
[9] Boraey MA, Hoe S, Sharif H, Miller DP, Lechuga-Ballesteros D, Vehring R. Improvement of the dispersibility of spray-dried budesonide powders using leucine in an ethanol–water cosolvent system. Powder Technol 2013;236:171–8.
[10] Simon A, Amaro MI, Cabral LM, Healy AM, de Sousa VP. Development of a novel dry powder inhalation formulation for the delivery of rivastigmine hydrogen tartrate. Int J Pharm 2016;501(1–2):124–38.
[11] Sou T, Kaminskas LM, Nguyen TH, Carlberg R, McIntosh MP, Morton DA. The effect of amino acid excipients on morphology and solid-state properties of multi-component spray-dried formulations for pulmonary delivery of biomacromolecules. Eur J Pharm Biopharm 2013;83(2):234–43.
[12] Bhardwaj R, Fang X, Somasundaran P, Attinger D. Self-assembly of colloidal particles from evaporating droplets: role of DLVO interactions and proposition of a phase diagram. Langmuir 2010;26(11):7833–42.
[13] Osman A, Goehring L, Patti A, Stitt H, Shokri N. Fundamental investigation of the drying of solid suspensions. Ind Eng Chem Res 2017;56(37):10506–13.
[14] Vehring R. Pharmaceutical particle engineering via spray drying. Pharm Res 2008;25(5):999–1022.
[15] Seville PC, Li HY, Learoyd TP. Spray-dried powders for pulmonary drug delivery. Crit Rev™ Therapeut Drug Carrier Syst 2007;24(4):307–60.
[16] Mondal R, Das A, Sen D, Satapathy DK, Basavaraj MG. Spray drying of colloidal dispersions containing ellipsoids. J Colloid Interface Sci 2019;511:242–50.
[17] Patel RP, Patel MP, Suthar AM. Spray drying technology: an overview. Indian J Sci Technol 2009;2(10):44–7.
[18] Mahajan HS, Gundare SA. Preparation, characterization and pulmonary pharmacokinetics of xyloglucan microspheres as dry powder inhalation. Carbohydr Polym 2014;102:529–36.
[19] Mei Jin Tan B, Liew CV, Chan LW, Heng PWS. Particle surface roughness–its characterisation and impact on dry powder inhaler performance. Pulmonary Drug Deliv: Adv Challenges 2015(Chapter 9):199–222.
[20] Hou S, Wu J, Li X, Shu H. Practical, regulatory and clinical considerations for development of inhalation drug products. Asian J Pharm Sci 2015;10(6):490–500.
[21] Idrees H, Zaidi SZJ, Sabir A, Khan RU, Zhang X, Hassan SU. A review of biodegradable natural polymer-based nanoparticles for drug delivery applications. Nanomaterials 2020;10(10):1970.
[22] Kean T, Thanou M. Biodegradation, biodistribution and toxicity of chitosan. Adv Drug Deliv Rev 2010;62(1):3–11.
[23] Amidi M, Mastrobattista E, Jiskoot W, Hennink WE. Chitosan-based delivery systems for protein therapeutics and antigens. Adv Drug Deliv Rev 2010;62(1):59–82.
[24] Grenha A, Al-Qadi S, Seijo B. Remuñán-López C. The potential of chitosan for pulmonary drug delivery. J Drug Deliv Sci Technol 2010;20(1):33–43.
[25] Rodrigues S, Dionísio M, Remunan Lopez C, Grenha A. Biocompatibility of chitosan carriers with application in drug delivery. J Funct Biomater 2012;3(3):615–41.
[26] Yi C, Tsai ML, Liu T. Spray-dried chitosan/acid/NaCl microparticles enhance saltiness perception. Carbohydr Polym 2017;172:246–54.
[27] Rasul RM, Muniandy MT, Zakaria Z, Shah K, Chee CF, Dabbagh A, et al. A review on chitosan and its development as pulmonary particulate anti-infective and anti-cancer drug carriers. Carbohydr Polym 2020;250:116800.
[28] Shaw RH, Sherman JM. The production of volatile fatty acids and carbon dioxid by propionic acid bacteria with special reference to their action in cheese. J Dairy Sci 1923;6(4):303–9.
[29] Yang MH, Choong YM. A rapid gas chromatographic method for direct determination of short-chain (C2–C12) volatile organic acids in foods. Food Chem 2001;75(1):101–8.
[30] Hooper DC, Jacoby GA. Topoisomerase inhibitors: fluoroquinolone mechanisms of action and resistance. Cold Spring Harb Perspect Med 2016;6(9):a025320.
[31] Pham TD, Ziora ZM, Blaskovich MA. Quinolone antibiotics. Medchemcomm 2019;10(10):1719–39.
[32] Ehsan Z, Clancy JP. Management of Pseudomonas aeruginosa infection in cystic fibrosis patients using inhaled antibiotics with a focus on nebulized liposomal amikacin. Future Microbiol 2015;10(12):1901–12.
[33] Stockmann C, Sherwin CM, Ampofo K, Spigarelli MG. Development of levofloxacin inhalation solution to treat Pseudomonas aeruginosa in patients with cystic fibrosis. Ther Adv Respir Dis 2014;8(1):13–21.
[34] Bhushan B. Surface roughness analysis and measurement techniques. In: Modern Tribology Handbook, 2; 2020. p. 79–150.
[35] Duparre A, Ferre-Borrull J, Gliech S, Notni G, Steinert J, Bennett JM. Surface characterization techniques for determining the root-mean-square roughness and power spectral densities of optical components. Appl Opt 2002;41(1):154–71.
[36] May S, Jensen B, Wolkenhauer M, Schneider M, Lehr CM. Dissolution techniques for *in vitro* testing of dry powders for inhalation. Pharm Res 2012;29(8):2157–66.
[37] Mitchell JP, Costa PA, Waters S. An assessment of an Andersen Mark-II cascade impactor. J Aerosol Sci 1988;19(2):213–21.
[38] Dunbar C, Mitchell J. Analysis of cascade impactor mass distributions. J Aerosol Med 2005;18(4):439–51.
[39] Velaga SP, Djuris J, Cvijic S, Rozou S, Russo P, Colombo G, Rossi A. Dry powder inhalers: an overview of the *in vitro* dissolution methodologies and their correlation with the biopharmaceutical aspects of the drug products. Eur J Pharm Sci 2018;113:18–28.
[40] Malamatari M, Charisi A, Malamataris S, Kachrimanis K, Nikolakakis I. Spray drying for the preparation of nanoparticle-based drug formulations as dry powders for inhalation. Processes 2020;8(7):788.
[41] Tirumkudulu MS. Buckling of a drying colloidal drop. Soft Matter 2018;14(36):7455–61.
[42] Lintingre E, Ducouret G, Lequeux F, Olanier L, Périé T, Talini L. Controlling the buckling instability of drying droplets of suspensions through colloidal interactions. Soft Matter 2015;11(18):3660–5.
[43] Sen D, Bahadur J, Mazumder S, Verma G, Hassan PA, Bhattacharya S, et al. Nanocomposite silica surfactant microcapsules by evaporation induced self assembly: tuning the morphological buckling by modifying viscosity and surface charge. Soft Matter 2012;8(6):1955–63.
[44] Du X, Qiao SZ. Dendritic silica particles with center-radial pore channels: promising platforms for catalysis and biomedical applications. Small 2015;11(4):392–413.
[45] Esparza Y, Ngo TD, Fraschini C, Boluk YJI, Research EC. Aggregate morphology and aqueous dispersibility of spray-dried powders of cellulose nanocrystals. Ind Eng Chem Res 2019;58(43):19926–36.
[46] Elversson J, Millqvist-Fureby A. Particle size and density in spray drying—effects of carbohydrate properties. J Pharm Sci 2005;94(9):2049–60.
[47] Pilcer G, Amighi K. Formulation strategy and use of excipients in pulmonary drug delivery. Int J Pharm 2010;392(1–2):1–19.
[48] Jalvandi J. Novel chemical and physical approaches for sustainable drug release from biodegradable electrospun nanofibres. RMIT University; 2016.
[49] Ferrero F, Periolatto M. Antimicrobial finish of textiles by chitosan UV-curing. J Nanosci Nanotechnol 2012;12(6):4803–10.

[50] Islan GA, Ruiz ME, Morales JF, Sbaraglini ML, Enrique AV, Burton G, et al. Hybrid inhalable microparticles for dual controlled release of levofloxacin and DNase: physicochemical characterization and *in vivo* targeted delivery to the lungs. J Mater Chem B 2017;5(17):3132–44.
[51] Semwal A, Singh BK, Archana D, Verma A, Dutta PK. Macromolecular chitosan/ciprofloxacin pro-drugs: synthesis, physico-chemical and biological assessment for drug delivery systems. J Polym Mater 2012;29(1):1–13.
[52] Schittny A, Huwyler J, Puchkov M. Mechanisms of increased bioavailability through amorphous solid dispersions: a review. Drug Deliv 2020;27(1):110–27.
[53] Chang SH, Chian CH. Plasma surface modification effects on biodegradability and protein adsorption properties of chitosan films. Appl Surf Sci 2013;282:735–40.
[54] Baghel S, Cathcart H, O'Reilly NJ. Polymeric amorphous solid dispersions: a review of amorphization, crystallization, stabilization, solid-state characterization, and aqueous solubilization of biopharmaceutical classification system class II drugs. J Pharm Sci 2016;105(9):2527–44.
[55] Van den Mooter G. The use of amorphous solid dispersions: a formulation strategy to overcome poor solubility and dissolution rate. Drug Discov Today: Technol 2012;9(2):e79–85.
[56] Bernier SP, Surette MG. Concentration-dependent activity of antibiotics in natural environments. Front Microbiol 2013;4:20.
[57] Mehta PP. Dry powder inhalers: upcoming platform technologies for formulation development. Ther Deliv 2019;10(9):551–4.
[58] Han CS, Kang JH, Kim YJ, Kim DW, Park CW. Inhalable nano-dimpled microspheres containing budesonide-PLGA for improved aerodynamic performance. Int J Nanomedicine 2022;17:3405–19.
[59] Peng T, Zhang X, Huang Y, Zhao Z, Liao Q, Xu J, Huang Z, et al. Nanoporous mannitol carrier prepared by non-organic solvent spray drying technique to enhance the aerosolization performance for dry powder inhalation. Sci Rep 2017;7(1):1–11.
[60] Inthavong K, Tu J, Ahmadi G. Computational modelling of gas-particle flows with different particle morphology in the human nasal cavity. J Comput Multiphase Flows 2009;1(1):57–82.
[61] Beratlis N, Balaras E, Squires K. Effects of dimples on laminar boundary layers. J Turbul 2014;15(9):611–27.
[62] Dal Negro RW. Dry powder inhalers and the right things to remember: a concept review. Multidiscip Respir Med 2015;10(1):1–4.
[63] Duret C, Wauthoz N, Merlos R, Goole J, Maris C, Roland I, et al. *In vitro* and *in vivo* evaluation of a dry powder endotracheal insufflator device for use in dose-dependent preclinical studies in mice. Eur J Pharm Biopharm 2012;81(3):627–34.
[64] Liu D, Xu S, Xiao H, Wang Z, Mao N, Zhou J, et al. Quantitative determination of unbound levofloxacin by simultaneous microdialysis in rat pancreas after intravenous and oral doses. J Pharm Pharmacol 2014;66(9):1215–21.
[65] Acton Q.A. Pseudomonas aeruginosa: new insights for the healthcare professional (2012 Edition). ScholarlyEditions.
[66] King P, Citron DM, Griffith DC, Lomovskaya O, Dudley MN. Effect of oxygen limitation on the *in vitro* activity of levofloxacin and other antibiotics administered by the aerosol route against Pseudomonas aeruginosa from cystic fibrosis patients. Diagn Microbiol Infect Dis 2010;66(2):181–6.